Analysis of $1/f$ Noise in Switched MOSFET Circuits

Hui Tian and Abbas El Gamal, *Fellow, IEEE*

***Abstract*—Analysis of $1/f$ noise in MOSFET circuits is typically performed in the frequency domain using the standard stationary $1/f$ noise model. Recent experimental results, however, have shown that the estimates using this model can be quite inaccurate especially for switched circuits. In the case of a periodically switched transistor, measured $1/f$ noise power spectral density (psd) was shown to be significantly lower than the estimate using the standard $1/f$ noise model. For a ring oscillator, measured $1/f$-induced phase noise psd was shown to be significantly lower than the estimate using the standard $1/f$ noise model. For a source follower reset circuit, measured $1/f$ noise power was also shown to be lower than the estimate using the standard $1/f$ model. In analyzing noise in the follower reset circuit using frequency-domain analysis, a low cutoff frequency that is inversely proportional to the circuit on-time is assumed. The choice of this low cutoff frequency is quite arbitrary and can cause significant inaccuracy in estimating noise power. Moreover, during reset, the circuit is not in steady state, and thus frequency-domain analysis does not apply.**

This paper proposes a nonstationary extension of the standard $1/f$ noise model, which allows us to analyze $1/f$ noise in switched MOSFET circuits more accurately. Using our model, we analyze noise for the three aforementioned switched circuit examples and obtain results that are consistent with the reported measurements.

***Index Terms*—$1/f$ noise, CMOS image sensor, nonstationary noise model, periodically switched circuits, phase noise, ring oscillator, time-domain noise analysis.**

I. Introduction

HISTORICALLY, $1/f$ noise in MOSFETs was of concern mainly in the design of low-frequency linear analog circuits such as bias circuits, audio amplifiers, etc. [1]. As CMOS technology scales down to the submicrometer regime, $1/f$ noise has become of greater concern in a wider range of circuit designs. Scaling has enabled the use of CMOS technology in many new applications such as radio-frequency (RF) circuits and CMOS image sensors. These circuits have been found to be quite sensitive to $1/f$ noise. Moreover, as mentioned in [2], MOSFET $1/f$ noise power increases rapidly with technology scaling. It is, therefore, becoming more important to accurately estimate the effect of $1/f$ noise for a wide variety of MOSFET circuits.

Analysis of $1/f$ noise in MOSFET circuits is typically performed using the well-established stationary $1/f$ noise model [3], [4], which henceforth will be referred to as the standard $1/f$ noise model. Recent experimental results, however, show that the estimates using this standard model can be quite inaccurate, especially for switched circuits. An important class of such circuits is periodically switched circuits, which are widely used in RF applications, such as switched capacitor networks, modulators and demodulators, and frequency converters. In the simplest case of a periodically switched transistor, it was shown that the measured drain voltage $1/f$ noise power spectral density (psd) [5]–[7] is much lower than the estimate using the standard $1/f$ noise model. Another example that has recently been receiving much attention is $1/f$-induced phase noise in CMOS oscillators [8]–[10]. Unlike the amplitude fluctuations, which can be practically eliminated by applying limiters to the output signal, phase noise cannot be reduced in the same manner. As a result, phase noise limits the available channels in wireless communication. Recent measurements [7] show that the $1/f$-induced phase noise psd in ring oscillators is much lower than the estimate using the standard $1/f$ noise model.

Yet another example of a switched circuit is the source follower reset circuit, which is often used in the output stage of a charge-coupled device (CCD) image sensor [11] and the pixel circuit of a CMOS active pixel sensor (APS) [12]. To find the output noise power due to $1/f$ noise, frequency-domain analysis is typically performed using the standard $1/f$ noise model. A low cutoff frequency f_L that is inversely proportional to the circuit on-time is used to obtain reasonable noise power estimates. The choice of this low cutoff frequency is quite arbitrary, however, and can cause significant inaccuracy in estimating noise power [13]. Moreover, during reset, the circuit is not in steady state and thus frequency-domain analysis does not apply.

In this paper, we propose a nonstationary extension of the standard $1/f$ noise model. We show that using this model, more accurate estimates of the effect of $1/f$ noise in switched circuits can be obtained. In particular, we consider the aforementioned three example circuits. For the reset circuit, we use our nonstationary model and time-domain analysis to find a more accurate estimate of the output $1/f$ noise power.

The rest of this paper is organized as follows. In Section II, we describe the standard stationary MOSFET $1/f$ noise model and our nonstationary extension. In Sections III–V, we use our nonstationary model to estimate the effect of $1/f$ noise on a periodically switched transistor, ring oscillator, and source-follower reset circuit, respectively. In all cases, we find that our estimates are consistent with the reported measurement results.

II. MOSFET $1/f$ Noise Models

A. Standard $1/f$ Noise Model

It is now widely believed that $1/f$ noise in a MOSFET is due to traps in the gate oxide [3], [4]. This is supported by studies of small-area submicrometer MOSFETs, where only a single trap

Manuscript received July 2000; revised January 2001. This work was supported in part by Agilent, Canon, HP, Interval Research, and Kodak under the Programmable Digital Camera Project. This paper was recommended by Associate Editor M. Kouwenhoven.

The authors are with the Information Systems Laboratory, Electrical Engineering Department, Stanford University, Stanford, CA 94305 USA (e-mail: huitian@isl.stanford.edu; abbas@isl.stanford.edu).

Publisher Item Identifier S 1057-7130(01)03046-4.

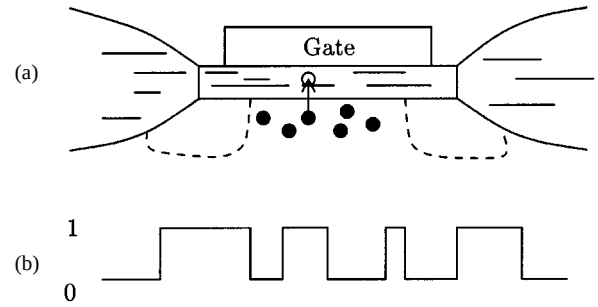

Fig. 1. (a) MOSFET with single trap in its gate oxide and (b) the resulting trapped electron number $N(t)$ waveform.

is active in the gate oxide. Capture and emission of channel carriers by this trap are represented by the trapped electron number $N(t)$, which takes a value of one if a carrier is captured and zero otherwise, as depicted in Fig. 1. The trap is active when its energy level is close to the Fermi level [14] in the bulk. In this case, the capture and emission rates must be nearly equal. Thus, $N(t)$ can be modeled as a random telegraph signal (RTS) with rate λ. In equilibrium, the autocovariance of $N(t)$ is given by

$$\mathcal{C}_\lambda(\tau) = \tfrac{1}{4}\, e^{-2\lambda\tau}$$

and the corresponding double-sided psd is

$$S_\lambda(f) = \frac{1}{4}\frac{\lambda}{\lambda^2 + (\pi f)^2}.$$

In practical MOSFETs there can be many traps in the gate oxide. Since each trap captures and emits carriers independently, the psd of the total trapped electron number is the sum of the psds for the individual trapped electron numbers. Traps can have different rates depending on their location in the gate oxide. The distribution of the rates is believed to obey a log uniform law [15]

$$g(\lambda) = \frac{4kTAt_{\rm ox}N_t}{\lambda \log\dfrac{\lambda_H}{\lambda_L}} \tag{1}$$

where

kT	thermal energy;
A	channel area;
$t_{\rm ox}$	effective gate-oxide thickness;
N_t	trap density (in $\mathrm{eV}^{-1}\mathrm{cm}^{-3}$);
λ_H	fastest transition rate or high corner frequency;
λ_L	slowest transition rate or low corner frequency.

The corner frequencies are related to $t_{\rm ox}$ through the equation $\log \lambda_H/\lambda_L = \gamma t_{\rm ox}$, where γ is the tunneling constant. The psd of the total trapped electron number is thus given by

$$\begin{aligned} S(f) &= \int_{\lambda_L}^{\lambda_H} S_\lambda(f) g(\lambda)\, d\lambda \\ &\approx \frac{kTAN_t}{2\gamma f}, \qquad \text{for } \lambda_L < f < \lambda_H. \end{aligned} \tag{2}$$

For $f < \lambda_L$, $S(f)$ is constant, and for $f > \lambda_H$, it is $\propto 1/f^2$.

The MOSFET charge-control analysis can then be used together with the derived psd of the total trapped electron number to find the $1/f$ noise psd of the gate voltage. For a submicrometer n-channel MOSFET, carrier number fluctuations dominate [16], [17] and the equivalent $1/f$ noise psd of the gate voltage is given by

$$S_{V_g}(f) = \frac{1}{C_{\rm ox}^2}\left(\frac{q}{A}\right)^2 S(f) = \frac{q^2 kTN_t}{2C_{\rm ox}^2 A\gamma f} = \frac{k_F}{2C_{\rm ox}Af} \tag{3}$$

where $C_{\rm ox}$ is the gate-oxide capacitance and k_F is the widely used SPICE $1/f$ noise parameter.

A unified number and mobility theory [3] can be used to extend these results to p-channel MOSFETs.

B. Nonstationary $1/f$ Noise Model

In this subsection, we present our nonstationary extension of the standard $1/f$ noise model discussed in the previous section. The main purpose of the extension is to be able to accurately analyze $1/f$ noise in switched circuits. We begin by considering the case of a single trap in an n-channel MOSFET. The key observation that led to our extension is that with very high probability, the trap is empty when the transistor is off. The physical reason can be explained via the MOSFET energy band diagram in Fig. 2. The energy levels E_t^o and E_t represent the trap energy in the off and on states, respectively. Note that for the trap to be active when the transistor is on, E_t must be very close to E_f, i.e., $E_t \approx E_f$. When the transistor is turned on, the trap energy shifts down by several hundred millivolts, which is the same as the shift in the surface potential. This is the case since the difference between the energy level of the trap and that of the oxide conduction band is independent of the gate bias voltage. This means that $E_t^o - E_t \gg kT$. It is well known [14] that the ratio of the trap capture rate λ_c to its emission rate λ_e is exponentially related to the difference between the trap energy and the Fermi level. When the transistor is off, this gives

$$\frac{\lambda_c}{\lambda_e} = \exp\left(\frac{E_F - E_t^o}{kT}\right) \ll 1.$$

Thus with very high probability, the trap is empty when the transistor is off. If we let $t = 0$ denote the time when the transistor turns on, we get that $N(0) \approx 0$.

Now let $p_1(t)$ be the probability that the trap is occupied at time $t > 0$. To find $p_1(t)$, we note that

$$p_1(t + \Delta t) = p_1(t)(1 - \lambda\Delta t) + (1 - p_1(t))\lambda\Delta t. \tag{4}$$

Thus in the limit

$$\frac{dp_1(t)}{dt} + 2\lambda p_1(t) = \lambda. \tag{5}$$

Solving for p_1, we find that

$$p_1(t) = \tfrac{1}{2}\left(1 - e^{-2\lambda t}\right). \tag{6}$$

The probability that the trap is occupied at time $t+\tau$, for $\tau > 0$, given that it is occupied at time t can be similarly found to be

$$p_{1,1}(t, \tau) = p_{1,1}(\tau) = \tfrac{1}{2}\left(1 + e^{-2\lambda\tau}\right). \tag{7}$$

Therefore, the autocovariance function of $N(t)$ is given by

$$\begin{aligned} \mathcal{C}_\lambda(t, \tau) &= p_1(t)p_{1,1}(\tau) - p_1(t)p_1(t+\tau) \\ &= \tfrac{1}{4}\, e^{-2\lambda\tau}\left(1 - e^{-4\lambda t}\right). \end{aligned} \tag{8}$$

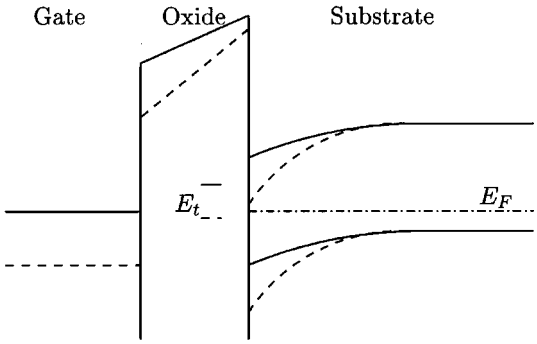

Fig. 2. Energy-band diagram for MOSFET, with an active trap inside its gate oxide. Solid lines are used when the transistor is off, and dashed lines are used when the transistor is on.

As $t \to \infty$, $\mathcal{C}_\lambda(t,\tau) \to 1/4\, e^{-2\lambda\tau}$, which is the stationary autocovariance function derived in the previous subsection.

The autocovariance of the total trapped electron number is simply the sum of the autocovariances for the individual traps in the gate oxide, i.e.,

$$\mathcal{C}(t,\tau) = \int_{\lambda_L}^{\lambda_H} \mathcal{C}_\lambda(t,\tau) g(\lambda)\, d\lambda.$$

Applying charge-control analysis, the equivalent gate voltage autocovariance function can be numerically evaluated.

For the examples in the following sections, we assume a 0.35-μm CMOS technology with $t_{\text{ox}} = 7$ nm, $\gamma = 10^8$ cm^{-1}, $\lambda_H = 10^{10}$ s^{-1}, and $N_t = 10^{17}$ eV^{-1}cm^{-3}. Using these parameter values, we get $\lambda_L = 4 \times 10^{-21}$, $C_{\text{ox}} = 5$ fF μm^{-2}, and $k_F = 5 \times 10^{-24}$ V^{2}F at $T = 300$K.

III. $1/f$ Noise in a Periodically Switched Transistor

Periodically switched circuits are widely used in RF applications, such as switched capacitor networks, modulators and demodulators, and frequency converters. In this section, we use our nonstationary $1/f$ noise model to analyze the simplest example of such circuits, the periodically switched transistor. Fig. 3 depicts a typical setup for measuring $1/f$ noise psd for a transistor. In the periodically switched case, the gate of the transistor is driven by a square wave voltage source that switched between 0 V and v_H, which is high enough to bias the transistor in the saturation region. Measured $1/f$ noise psd using this setup was reported in [5]–[7]. These papers comment on the fact that the measured psd is significantly lower than the psd estimated using the standard $1/f$ model. We now show that the psds estimated using our nonstationary model are more consistent with the measurement results.

We first consider a single active trap. Using (8), we can write the autocovariance function of the trapped electron number as

$$\mathcal{C}_\lambda(t,\tau) = \begin{cases} \frac{1}{4} e^{-2\lambda\tau}\left(1 - e^{-4\lambda(t-nT)}\right), & nT \le t, \\ & t+\tau \le nT + \dfrac{T}{2} \\ 0 & \text{otherwise.} \end{cases} \tag{9}$$

Note that $\mathcal{C}_\lambda(t,\tau)$ is periodic in t and that the trapped electron number is a wide sense cyclostationary process. As proved in [18]–[20], low-pass filtering or bandpass filtering of a wide sense cyclostationary process results in a wide sense stationary process when the filter bandwidth is less than half the switching frequency $1/T$. Spectrum analyzers normally perform this conversion before the spectrum is determined. Therefore, the autocovariance of the resulting stationary process can be obtained by averaging the time-varying autocovariance over one cycle

$$\mathcal{C}^s_\lambda(\tau) = \frac{1}{T}\int_0^T \mathcal{C}_\lambda(t,\tau)\, dt = \left(\frac{1}{2} - \frac{1 - e^{-2\lambda T}}{4\lambda T}\right)\frac{1}{4}\, e^{-2\lambda\tau}. \tag{10}$$

Note that the standard $1/f$ noise model gives $\mathcal{C}^s_\lambda(\tau) = (1/2)\,(1/4)\, e^{-2\lambda\tau}$ and thus predicts the psd curve to be 3 dB lower at all frequencies than a dc-biased transistor.

Now performing Fourier transform on $\mathcal{C}^s_\lambda(\tau)$, and summing over the contributions of all active traps, we find the drain $1/f$ noise voltage psd

$$\begin{aligned} S_{V_d}(f) &= \xi_V S(f) \\ &= \xi_V \int_{\lambda_L}^{\lambda_H} g(\lambda)\left(\frac{1}{2} - \frac{1 - e^{-2\lambda T}}{4\lambda T}\right)\frac{1}{2}\frac{\lambda}{\lambda^2 + (\pi f)^2}\, d\lambda \end{aligned} \tag{11}$$

where ξ_V relates the trapped electron number psd to the drain noise voltage psd.

Fig. 4 plots the simulated drain $1/f$ noise voltage psd for both the standard and the nonstationary $1/f$ noise models assuming switching frequency of 2 MHz. For comparison, we also plot the drain $1/f$ noise voltage psd for the dc-biased transistor. Note that for f much higher than the switching frequency, the two models yield the same result, which, as pointed out, is 3 dB lower than the noise psd in the dc biased case. For f lower than the switching frequency, the two models deviate significantly. The standard model still predicts noise psd to be 3 dB lower than the dc-biased case, while the nonstationary model predicts further noise psd reduction that increases as f decreases. This is consistent with the behavior of the measured psd.

IV. $1/f$-Induced Phase Noise in a Ring Oscillator

The phase noise in CMOS oscillators has recently been receiving much attention [8]–[10] since it sets a limit on the available channels in wireless communication. It is typically represented by sideband noise power spectral density

$$\mathcal{L}(\Delta\omega) = 10\log\frac{\mathcal{P}(\omega_0 + \Delta\omega,\ 1\ \text{Hz})}{\mathcal{P}(\omega_0)}$$

where $\mathcal{P}(\omega_0 + \Delta\omega,\ 1\ \text{Hz})$ represents the sideband power at frequency offset of $\Delta\omega$ from the carrier frequency ω_0 with a measurement bandwidth of 1 Hz. Computing this number requires knowledge of how the device noise current is converted into oscillator output voltage. In [9], this is done in two steps. The first step involves the conversion of excess injected current into excess phase, which is done via a linear time-varying system (LTVS). The second step is phase modulation, where the excess

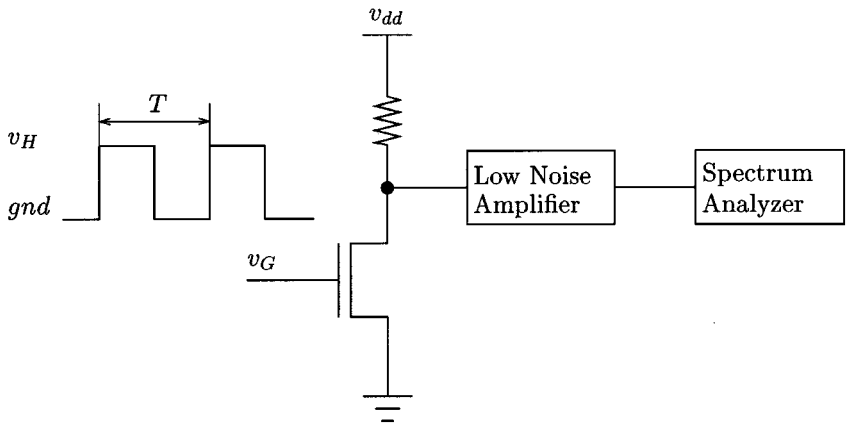

Fig. 3. Spectrum analysis of a periodically switched nMOS transistor.

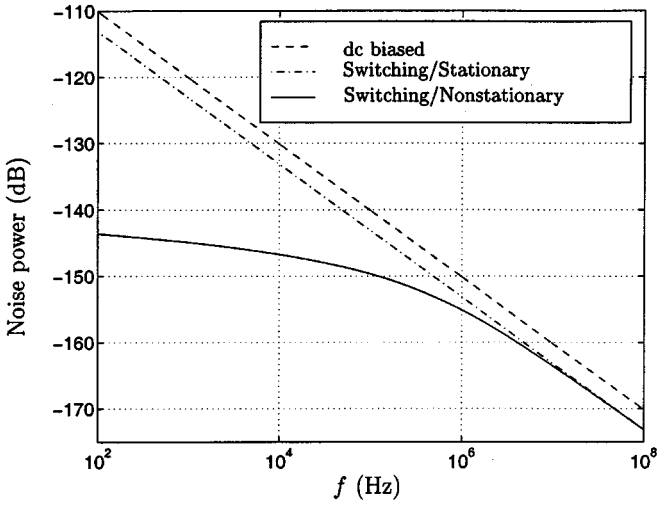

Fig. 4. Simulated $1/f$ noise psd for switched and dc biased transistors.

phase is converted into voltage. The LTVS is characterized by its impulse response

$$h(t,\tau)=\frac{\Gamma(\omega_0\tau)}{q_{\max}}u(t-\tau)$$

where

$q_{\max}$ maximum charge displacement;
u unit step function;
Γ periodic impulse sensitivity function (ISF).

Expanding

$$\Gamma(\omega_0\tau)=\frac{c_0}{2}+\sum_{n=1}^{\infty}c_n\cos(n\omega_0\tau+\theta_n)$$

and assuming excess injected current due to $1/f$ noise with single-sided psd $(g_m^2\pi k_F)/(C_{\rm ox}A\Delta\omega)$, it can be shown that

$$\mathcal{L}(\Delta\omega)=10\log\left(\frac{c_0^2g_m^2\pi k_F}{8q_{\max}^2C_{\rm ox}A}\frac{1}{\Delta\omega^3}\right). \tag{12}$$

This approach, however, cannot be used to explain the abnormal reduction in phase noise when the transistors in a ring oscillator are periodically turned on and off [7]. We now show that using our nonstationary $1/f$ noise model, we can explain this reduction. In these experiments, one transistor typically has much smaller area than the rest, and thus its $1/f$-induced phase noise dominates. To study the noise due to this transistor, we first consider the case where there is only one active trap inside its gate oxide. Using the periodic autocovariance function of the trapped electron number as expressed in (9), we can find the time-varying psd [21]

$$S(t,f)=\begin{cases}\dfrac{1}{2}\dfrac{\lambda}{\lambda^2+(\pi f)^2}\left(1-e^{-4\lambda(t-nT)}\right), & nT\le t,\\ & t+\tau\le nT+\dfrac{T}{2}\\ 0, & \text{otherwise}\end{cases} \tag{13}$$

where $T=(2\pi)/\omega_0$. Note that the function $S(t,f)$ is separable and can thus be expressed as $S(f)\alpha(\omega_0 t)$, where $S(f)=1/2\,\lambda/(\lambda^2+(\pi f)^2)$ and $\alpha(\omega_0 t)$ is a periodic function. For this class of cyclostationary noise sources, it is shown in [9] that phase noise can still be calculated using (12), with $S(f)$ representing a stationary noise source that is associated with an effective ISF $\Gamma_{\rm eff}=\Gamma(\omega_0 t)\alpha(\omega_0 t)$. In [9], it is also shown that for independent noise sources, the total phase noise is simply the sum of the phase noise due to each source. We can use this fact to find the $1/f$-induced phase noise psd in the case of many traps, since their trapped electron numbers are independent.

To demonstrate that our nonstationary $1/f$ noise model can be used to explain the reduction in phase noise, consider a ring oscillator with the ISF shown in Fig. 5. The figure also plots the gate voltage for the transistor under consideration. Fig. 6 plots the simulated phase noise psd using both the nonstationary and the standard $1/f$ noise models at 2 MHz switching frequency. We also plot the phase noise psd of a nonswitching ring oscillator, where the transistor is always on. As can be seen, the standard $1/f$ noise model reports phase noise that is 6 dBc lower than the nonswitching case, at all frequencies. The 6 dBc reduction, however, is too small when compared to the reported measurements [7], which show over 10 dBc reduction in the 1–10 kHz range. By comparison, the plot using our nonstationary model shows 10–20 dBc reduction in this frequency range. The reduction is the result of the decrease in $1/f$ noise due to the switching of the transistor, as discussed in the previous section. Note that our model predicts an increase in $1/f$-induced phase noise above 100 kHz relative to the estimates of the standard

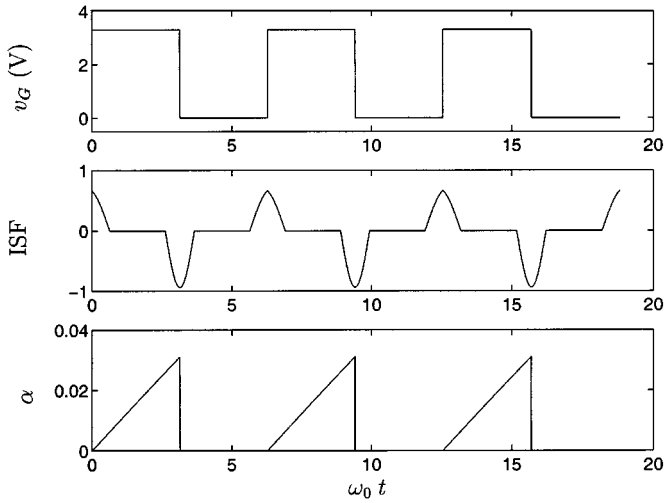

Fig. 5. (a) The gate voltage of the dominant nMOS transistor in a ring oscillator and (b) the associated ISF, and $\alpha(\omega_0 t)$ for $\lambda = 31.6$ kHz.

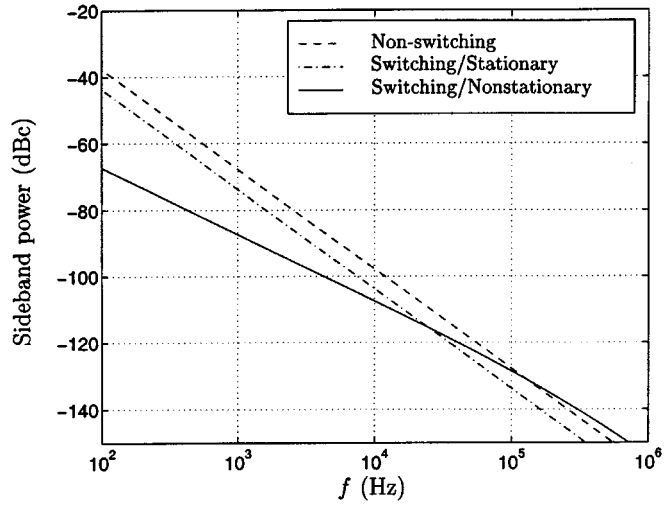

Fig. 6. Simulated $1/f$-induced phase noise psd for a ring oscillator.

model. This, we believe, is due to the nonflat shape of the $\alpha(\omega_0 t)$ as shown in Fig. 5, which can cause significant asymmetry in the effective ISF Γ_{eff}, and thus can increase phase noise.

V. $1/f$ Noise in Source Follower Reset Circuit

The source follower reset circuit is commonly used in the output stage of a CCD image sensor and the pixel circuit of a CMOS APS. As depicted in Fig. 7 during reset, the gate of the transistor is set to a high voltage v_{reset} for a short period of time t_r. To find the output noise power due to the transistor $1/f$ noise, frequency-domain analysis is typically performed using the standard $1/f$ noise model to get

$$\overline{V_{\text{out}}^2(t_r)} = \int_{1/t_r}^{\infty} \frac{S_{I_d}(f)}{g_m^2(t_r) + 4\pi^2 f^2 C^2}\, df$$

where g_m is the transistor transconductance and S_{I_d} is the transistor drain current $1/f$ noise psd. The choice of $1/t_r$ as a low cutoff frequency is quite arbitrary, however. Moreover, the circuit is not in steady state [22], and thus it is not appropriate to use frequency-domain analysis.

In this section, we use our nonstationary $1/f$ noise model and time-domain analysis to obtain more accurate noise power estimates. First note that at the beginning of reset, the transistor is operating either in the saturation region or in subthreshold depending on the value of v_{out}. Even if the transistor is first in saturation, it quickly goes into subthreshold and does not reach steady state. This was explained in detail in [22], where we analyzed reset noise due to thermal and shot noise sources. The circuit noise model during reset is shown in Fig. 7(b). The current source $I_d(t)$ models the transistor $1/f$ noise, and g_m is the transistor transconductance in subthreshold, which is time varying. The output noise voltage at the end of reset is given by [22]

$$V_{\text{out}}(t_r) = \int_0^{t_r} \frac{I_d(s)}{C} \exp\left(-\int_s^{t_r} \frac{g_m(\tau)}{C}\, d\tau\right) ds. \quad (14)$$

The output reset noise power is thus given by

$$\overline{V_{\text{out}}^2(t_r)} = \left(\frac{q}{AC_{\text{ox}}C}\right)^2 \int_0^{t_r}\int_0^{t_r} g_m(s_1) g_m(s_2) \cdot \mathcal{C}(s_1, |s_2 - s_1|) \exp\left(-\frac{1}{C}\int_{s_1}^{t_r} g_m(\tau_1)\, d\tau_1\right) \cdot \exp\left(-\frac{1}{C}\int_{s_2}^{t_r} g_m(\tau_2)\, d\tau_2\right) ds_1\, ds_2. \quad (15)$$

Using the MOS transistor subthreshold I–V characteristics, we get that $g_m(\tau) \approx C/(\tau + \delta)$, where δ is the thermal time [22]. Thus

$$\exp\left(-\frac{1}{C}\int_s^{t_r} g_r(\tau)\, d\tau\right) \approx \frac{s+\delta}{t_r+\delta}.$$

Substituting this and (1) and (8) into (15), we get that

$$\overline{V_{\text{out}}^2(t_r)} = \left(\frac{q}{AC_{\text{ox}}}\right)^2 \frac{1}{(t_r+\delta)^2} \int_0^{t_r}\int_0^{t_r}\int_{\lambda_L}^{\lambda_H} \cdot \mathcal{C}_\lambda(s_1, |s_2 - s_1|) g(\lambda)\, d\lambda\, ds_1\, ds_2. \quad (16)$$

Note that this result is virtually independent of the capacitance. This of course is very different from the famous kT/C reset noise due to thermal and shot noise sources. The reason is that $1/f$ noise power is concentrated on low frequencies, and thus is less sensitive to circuit bandwidth and hence C.

In Fig. 8, we compare the results using our method to the results using conventional frequency-domain analysis. To perform the frequency-domain analysis, we need to decide on the value of g_m to use. In that figure, we plot the results of the frequency-domain analysis for two values of g_m, one at the beginning and the other at the end of the reset time. Note the enormous difference between the curves for the two g_m values. Depending on which g_m value is used, the results can vary from 3.2 to 68 μV at $t_r = 10$ μs. This presents yet another serious shortcoming of using frequency-domain analysis.

To isolate the effect of using the standard versus the nonstationary noise models, in Fig. 9 we plot the curves for both models using the same time-varying circuit model. In calculating the noise assuming the standard model, we simply replace the $\mathcal{C}_\lambda(s_1, |s_2 - s_1|)$ in (16) by the stationary autocovariance $\mathcal{C}_\lambda(|s_2 - s_1|)$. As can be seen from the two curves, the root mean square (rms) noise voltage using the standard model is

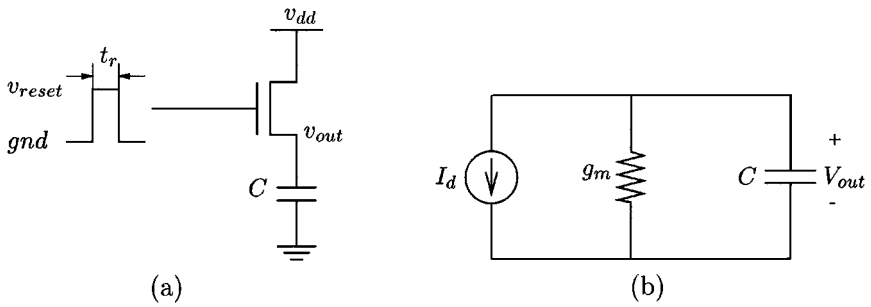

Fig. 7. (a) Source follower reset circuit and (b) its noise model during reset.

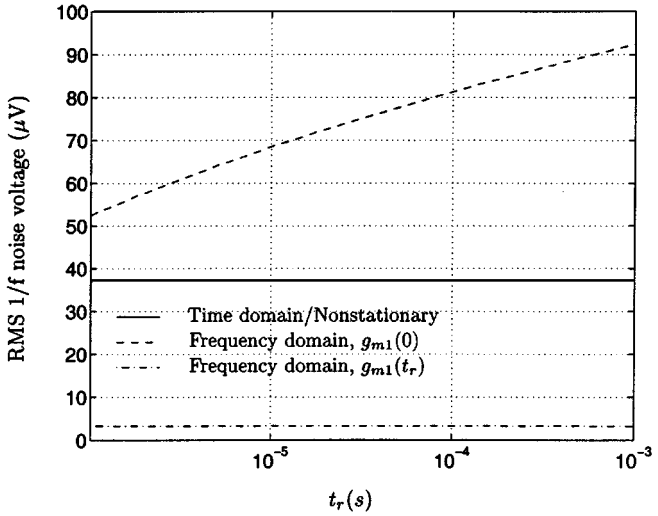

Fig. 8. Simulated output referred rms $1/f$ reset noise using frequency-domain analysis versus using our method.

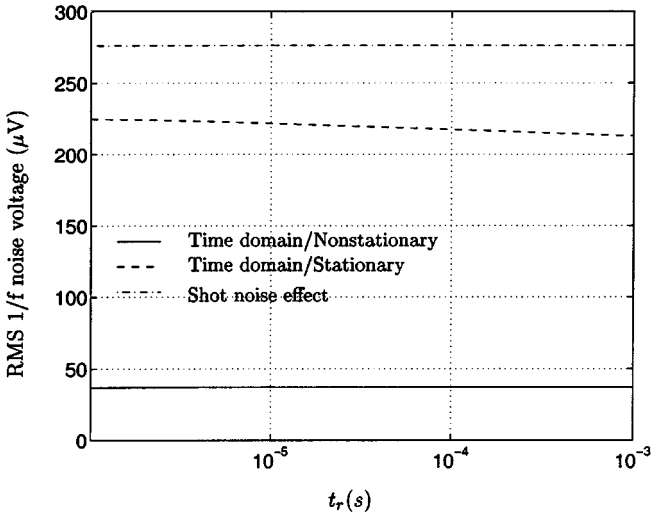

Fig. 9. Simulated output referred rms $1/f$ reset noise using standard $1/f$ noise model versus using the nonstationary extension, both assuming time-varying circuit model.

much higher, e.g., 222 versus 37.2 μV at $t_r = 10$ μs. The noise due to reset transistor shot noise is also plotted and is around 276 μV. Note that the rms $1/f$ noise voltage predicted by the standard model is comparable to the effect of the shot noise. Measurement results [22], [23] show, however, that shot noise dominates the reset noise, which corroborates the analysis using our method.

VI. Conclusion

Recent experimental results showed that the estimates of the effect of $1/f$ noise obtained using the standard $1/f$ noise model can be quite inaccurate, especially for switched circuits. In the case of a periodically switched transistor, measured $1/f$ noise psd was shown to be significantly lower than the estimate using the standard $1/f$ noise model. Similarly, measured $1/f$-induced phase noise psd in a ring oscillator was also shown to be significantly lower than the estimates using the standard $1/f$ noise model. To find the output noise power due to $1/f$ noise in a source follower reset circuit, frequency-domain analysis is typically performed using the standard $1/f$ noise model. A low cutoff frequency that is inversely proportional to the circuit on-time is typically used to obtain reasonable noise power estimates. The choice of this low cutoff frequency is quite arbitrary, however, and can cause significant inaccuracy in estimating noise power. Moreover, during reset the circuit is not in steady state and thus frequency-domain analysis does not apply. We used our nonstationary extension of the standard $1/f$ noise model to analyze the effect of $1/f$ noise in these three switched circuit examples. In all cases, we obtained results that are more consistent with reported measurements than those obtained using the standard $1/f$ noise model. This not only validates our model but also means that accurate estimates of the effect of $1/f$ noise on MOSFET circuits can now be obtained for a wider range of applications.

Acknowledgment

The authors would like to thank T. Chen, S. H. Lim, X. Liu, and K. Salama for the helpful discussions.

References

[1] P. R. Gray and R.G. Meyer, *Analysis and Design of Analog Integrated Circuits*. New York: Wiley, 1993.
[2] C. Hu, G. P. Li, E. Worley, and J. White, "Consideration of low-frequency noise in MOSFET's for analog performance," *IEEE Electron Device Lett.*, vol. 17, pp. 552–554, Dec. 1996.
[3] K. K. Hung, P. K. Ko, C. Hu, and Y. C. Cheng, "A unified model for the flicker noise in metal-oxide-semiconductor field-effect transistors," *IEEE Trans. Electron Devices*, vol. 37, pp. 654–665, Mar. 1990.
[4] C. Jakobson, I. Bloom, and Y. Nemirovsky, "$1/f$ noise in CMOS transistors for analog applications from subthreshold to saturation," *Solid-State Electron.*, vol. 42, no. 10, pp. 1807–1817, 1998.
[5] I. Bloom and Y. Nemirovsky, "$1/f$ noise reduction of metal-oxide-semiconductor transistors by cycling from inversion to accumulation," *Appl. Phys. Lett.*, vol. 58, no. 15, pp. 1664–1666, Apr. 1991.

[6] B. Dierickx and E. Simoen, "The decrease of 'random telegraph signal' noise in metal–oxide-semiconductor field-effect transistors when cycled from inversion to accumulation," *J. Appl. Phys.*, vol. 71, no. 4, pp. 2028–2029, Feb. 1992.
[7] S. L. J. Gierkink, E. A. M. Klumperink, A. P. van der Wel, G. Hoogzaad, E. van Tuijl, and B. Nauta, "Intrinsic $1/f$ device noise reduction and its effect on phase noise in CMOS ring oscillators," *IEEE J. Solid-State Circuits*, vol. 34, pp. 1022–1025, July 1999.
[8] A. Hajimiri, S. Limotyrakis, and T. H. Lee, "Jitter and phase noise in ring oscillators," *IEEE J. Solid-State Circuits*, vol. 34, pp. 790–804, June 1999.
[9] A. Hajimiri and T. H. Lee, "A general theory of phase noise in electrical oscillators," *IEEE J. Solid-State Circuits*, vol. 33, pp. 179–194, Feb. 1998.
[10] B. Razavi, "A study of phase noise in CMOS oscillators," *IEEE J. Solid-State Circuits*, vol. 31, pp. 331–343, Mar. 1996.
[11] A. J. P. Theuwissen, *Solid-State Imaging with Charge-Coupled Devices*. Norwell, MA: Kluwer Academic, 1995.
[12] E. R. Fossum, "CMOS image sensors: Electronic camera-on-a-chip," *IEEE Trans. Electron Devices*, vol. 44, pp. 1689–1698, Oct. 1997.
[13] H. Tian and A. El Gamal, "Analysis of $1/f$ noise in CMOS APS," in *Proc. SPIE*, vol. 3965, San Jose, CA, Jan. 2000.
[14] M. J. Kirton and M. J. Uren, "Noise in solid-state microstructures: A new perspective on individual defects, interface states and low-frequency ($1/f$) noise," *Adv. Phys.*, vol. 38, no. 4, pp. 367–468, 1989.
[15] A. van der Ziel, *Noise in Solid State Devices and Circuits*. New York: Wiley, 1986.
[16] J. Chang, A. A. Abidi, and C. R. Viswanathan, "Flicker noise in CMOS transistors from subthreshold to strong inversion at various temperatures," *IEEE Trans. Electron Devices*, vol. 41, pp. 1965–1971, Nov. 1994.
[17] T. Boutchacha, G. Ghibaudo, G. Guegan, and T. Skotnicki, "Low frequency noise characterization of 0.18 um Si CMOS transistors," *Microelectron. Reliab.*, vol. 37, no. 10/11, pp. 1599–1602, 1997.
[18] T. Strom and S. Signell, "Analysis of periodically switched linear circuits," *IEEE Trans. Circuits Syst.*, vol. 24, pp. 531–541, Oct. 1977.
[19] C. D. Hull and R. G. Meyer, "A systematic approach to the analysis of noise in mixers," *IEEE Trans. Circuits Syst.*, vol. 40, pp. 909–919, Dec. 1993.
[20] J. Roychowdhury, D. Long, and P. Feldmann, "Cyclostationary noise analysis of large RF circuits with multitone excitations," *IEEE J. Solid-State Circuits*, vol. 33, pp. 324–336, Mar. 1998.
[21] D. G. Lampard, "Generalization of the Wiener–Khintchine theorem to nonstationary processes," *J. Appl. Phys.*, vol. 25, no. 6, pp. 802–803, June 1954.
[22] H. Tian, B. Fowler, and A. El Gamal, "Analysis of temporal noise in CMOS APS," in *Proc. SPIE*, vol. 3649, San Jose, CA, Jan. 1999, pp. 177–185.
[23] R. Sarpeshkar, T. Delbruck, and C. A. Mead, "White noise in MOS transistors and resistors," *IEEE Circuits Devices Mag.*, vol. 9, pp. 23–29, Nov. 1993.

Hui Tian received the B.S. degrees in applied physics and business administration and the M.S. degree in accelerator physics from Tsinghua University, Beijing, China, in 1993 and 1996, respectively, and the M.S. degree in electrical engineering and the Ph.D. degree in applied physics from Stanford University, Stanford, CA, in 1999 and 2000, respectively.

He is presently working at Pixim, Inc., Mountain View, CA, where he is developing CMOS image sensors.

Abbas El Gamal (S'71–M'73–SM'83–F'00) received the B.S. degree in electrical engineering from Cairo University in 1972 and the M.S. degree in statistics and the Ph.D. degree in electrical engineering from Stanford University, Stanford, CA, in 1977 and 1978, respectively.

From 1978 to 1980, he was an Assistant Professor of Electrical Engineering at the University of Southern California. He joined the Stanford faculty in 1981, where he is currently a Professor of Electrical Engineering. From 1984 to 1988, while on leave from Stanford, he was Director of LSI Logic Research Lab, then co-founder and Chief Scientist of Actel Corporation. From 1990 to 1995, he was a co-founder and Chief Technical Office of Silicon Architects, which currently part of Synopsys. He is currentlly the Principal Investigator on the Stanford Programmable Digital Camera project. His research interests include CMOS image sensors and digital cameras, image processing, FPGAs, VLSI CAD, and network information theory. He has authored or co-authored over 100 papers and 20 patents in these areas. He serves on the Board of Directors and Advisory Boards of several IC and CAD companies.

Dr. El Gamal is a member of the ISSCC Technical Program Committee.